RSC Advances

PAPER

Evolution of excitation wavelength dependent photoluminescence in nano-CeO_2 dispersed ferroelectric liquid crystals

Cite this: *RSC Adv.*, 2014, **4**, 11351

Puja Goel,*[a] Manju Arora[b] and A. M. Biradar[b]

The optical properties of nano-ceria (nano-CeO_2) dispersed ferroelectric liquid crystals (FLCs) have been investigated by excitation wavelength dependent photoluminescence (PL) spectroscopy. The PL spectra of nano-ceria exhibited a strong excitation wavelength dependence in the 255–370 nm range. The red shift in the violet emission band of ceria *i.e.* from 368 nm to 396 nm with increasing excitation wavelength, has been attributed to the recombination of electrons trapped in the defect band and the deeply trapped holes in oxygen vacancies. This excitation wavelength dependence of ceria has noticeably been manifested in the PL response of FLC–CeO_2 nanocomposites as well. PL emission recorded at an excitation wavelength where host and guest materials show intense emission, *i.e.* 340 nm, exhibits a quenching effect connected to the overlapping of emission and absorption bands of the host FLC and guest ceria NPs respectively. No blue/red shift in the spectral energy band was observed at 310 and 340 nm excitations. On the other hand, emission spectra at a lower excitation wavelength followed a reverse trend: an increase in the emission intensity, with a large blue shift in spectral energy band. The mechanisms involved in the changes of the PL spectrum of FLC–ceria nanocomposites with varying ceria concentration and excitation wavelengths are discussed in detail.

Received 2nd December 2013
Accepted 7th January 2014

DOI: 10.1039/c3ra47225f

www.rsc.org/advances

Introduction

The potential applications of ferroelectric liquid crystals (FLCs) in optical storage devices, flat panel displays, luminescent liquid crystal displays, spatial light modulators and electro-optic memories has led to a great deal of research over the past few decades owing to their bistability and faster switching response in comparison to conventional nematic liquid crystals. The use of nanomaterials, quantum dots *etc.* in liquid crystal (LC) science has further revived the hopes of researchers who have been looking for performance enhancement as well as finding new applications of prospective FLC based devices. Dispersing an appropriate amount of nanomaterials in FLCs not only enhances the physical properties of host FLCs but also can impart novel properties in nanocolloids/nanocomposites. In addition to this, nanomaterials and quantum dots have also played an important role in bringing forward LC materials for application in luminescent display devices.[1–4] In general, LC displays have comparatively low brightness and energy efficiency due to the use of polarizers and absorbing colored filters in their construction. They mostly fluoresce in the blue region of visible spectrum as a broad emission band which is the main limitation in the development of a full-color emissive LC display. Since a display device requires blue, green and red emitting liquid crystalline matrices without overlapping their emission bands, to improve the color performance of LCs, luminescent LC materials have been found to be promising for fabricating emissive type displays. To achieve this, sheets of photoluminescent material in LCs have been used as an active color filter. However, new research trends revolve around the application potential of nanomaterials/quantum dots for imparting photoluminescence (PL) in LC materials, taking into consideration the preliminary results reported so far.[1–6] For example, (a) gold nanoparticles (NPs) were found to increase the PL emission intensity of deformed helix FLC materials by nine fold,[1] (b) the emission profile of nematic LCs was strongly influenced in the presence of dye molecules[5] and (c) the enhancement and quenching of PL has also been reported for LCs doped with silver NPs.[6] In addition to this, the rare earth materials containing liquid crystals also follow the guest–host effect for optimizing the luminescent and liquid crystalline properties of the system independently.[7] The rare earth ions exist mostly in a trivalent state and form three types of complexes depending upon metal-to-ligand ratio: (i) tris-complexes, (ii) Lewis base adducts of tris-complexes and (iii) tetrakis complexes. Rare earth oxide ceria (CeO_2) is a wide energy band gap semiconductor (*e.g.* ~5.5 eV) with a fluorite structure and has attracted a great deal of attention for its tunable electronic and optical characteristics.[8] It is extensively

[a]*Division of Agricultural Chemicals, Indian Agricultural Research Institute, New Delhi 110012, India. E-mail: pujagoel@gmail.com*

[b]*Liquid Crystal Group, CSIR - National Physical Laboratory, Dr K. S. Krishnan Marg, New Delhi 110012, India*

considered in the field of luminescence, semiconductor devices, fuel cells and solar cells due to its chemical stability, high oxygen storage capacity and can easily shift between Ce^{4+} and Ce^{3+} oxidation states.[8–10] Owing to these remarkable features, we have dispersed nano-ceria in FLCs and characterized their photoluminescence response in terms of varying ceria concentration and wavelength of PL excitation.

Experimental

A suspension of ceria NPs (Sigma Aldrich) was obtained by dispersing the NPs in Millipore water (1 : 100) followed by one hour of ultrasonication. Selected amounts of this suspension (0.5, 1 and 5 μl) were added to a fixed amount of FLC material (3 mg) at 25 ± 2 °C in order to obtain the FLC–ceria nanocomposites. These mixtures were heated at 120 °C for 10 minutes followed by rigorous mixing. This heating and mixing process was repeated three times to ensure the complete removal of water. The mixtures were cooled to room temperature (25 ± 2 °C) and placed on one of the openings of the electro-optic cells. The cells were then kept in an oven at a 120 °C (slightly above the nematic to isotropic transition temperature of the FLC material *i.e.* 114.5 °C) for 20 minutes so that the material flowed inside the cell through capillary action. The samples were slowly cooled inside the oven and taken out when oven temperature reached 25 ± 2 °C.

The electro-optic cells were fabricated for textural and optical investigation by etching a square patterned electrode on an indium tin oxide ((ITO), resistivity ∼30 Ω μ^{-1}) coated glass substrate using photolithography. A cell thickness of ∼4 μm was maintained using Mylar spacers. The phase sequence of the investigated FLC, *i.e.* KCFLC 7s, is as follows:where Cryst., SmC*, SmA, N*, and Iso., represent crystal, chiral smectic C, smectic A, chiral nematic, and isotropic phases, respectively. For characterization of ceria NPs, High Resolution Transmission Electron Microscopy (HRTEM) was performed using the Tecnai G2F30 S-Twin (FEI; Super Twin lens with C s 1.2 mm) instrument with a point resolution of 0.2 nm and a lattice resolution of 0.14 nm. The samples for HRTEM analysis were prepared by dispersing the ceria NPs in acetone through ultrasonication and drying a droplet of the dispersion on a carbon coated copper grid at room temperature (25 ± 2 °C). A high-resolution polarizing optical microscope (POM, Carl Zeiss, Axioskop-40, Germany) equipped with a computer controlled charge coupled device (CCD) camera was used to investigate the optical textures of the pure and FLC–ceria NP dispersions. The photoluminescence spectra of pure and ceria dispersed samples were recorded using a Fluorolog (Jobin Yvon – Horiba, model-3-11) spectrofluorometer. A Shimadzu UV-Vis spectrophotometer (model no. UV-2401 PV) was used to record the UV-Vis absorption spectrum of the pure materials as well as the nanocomposites in the 200 nm–800 nm range.

Results and discussion

The HRTEM micrograph in Fig. 1(a) reveals that octahedral shaped ceria NPs have an average size of ∼18.5 nm with a very narrow size distribution. The size distribution of nanoparticles can also be seen through the histogram derived from the TEM picture of ceria NPs (Fig. 1(b)). The distribution can be well-fitted by the log normal distribution function[11]

$$y = y_0 + \frac{A}{w \times x\sqrt{2\pi}} \exp\left(-\frac{\left(\ln\left(\frac{x}{x_c}\right)\right)^2}{2 \times w^2}\right)$$

where "w" represents the standard deviation and "x_c" is the mean particle size.

In Fig. 1(c), the image of a single octahedron clearly shows that the edges are sharp and the lattice planes are well aligned. Furthermore, when looking at the textural changes in the FLC material in the presence of secondary phase ceria NPs, the bright (B) and scattered (S) state of the pure and dispersed NP samples were analyzed by obtaining high resolution optical micrographs under a crossed polarizer. As it is evident from Fig. 2, the homogenous alignment is retained with the addition of up to 5 μl of ceria NPs and that the NPs were uniformly dispersed within the FLC material.

So far, reports pertaining to the PL evolution in FLC based composites are predominantly focused on the PL intensity variations with dopant addition. In these investigations, our focus is to understand the mechanism of the excitation energy dependent PL emission (since dopants exhibit strong excitation dependence) in terms of the change in local field and coupling between the excitons of ceria nanoparticles and FLC molecules.

The PL spectra of the pure FLC and ceria nanoparticles were recorded at different excitation wavelengths in the range of 255 nm–370 nm. In Fig. 3(a), the PL spectra of the pure FLC show a broad absorption in the region 325 nm–575 nm with the peak maxima at ∼396 nm. The submerged components present in the broad asymmetric PL emission of the pure FLC at ∼396 nm were determined using Gaussian fitting. As shown in Fig. 3(b) three discrete submerged components with maxima at 380 nm, 412 nm and 446 nm could be resolved due to the luminance of the *trans*-isomer (π, π*), *cis*-isomer (n, π*) transitions and the intermediate conformation of excited *trans* isomers respectively.[12–14] Furthermore, it can be seen that the intensity of the PL emission signal increases in the 255 nm to 340 nm excitation wavelength range and then reduces drastically on further increasing the excitation wavelength to 370 nm. The peak ∼396 nm (ultraviolet emission) with submerged components in the FLC is due to the radiative relaxation of electrons from the lowest energy unoccupied molecular orbital (LUMO) to the highest energy occupied molecular orbital (HOMO) levels in the FLC. The uniform surface morphology with minor surface defects in the FLC leads to the

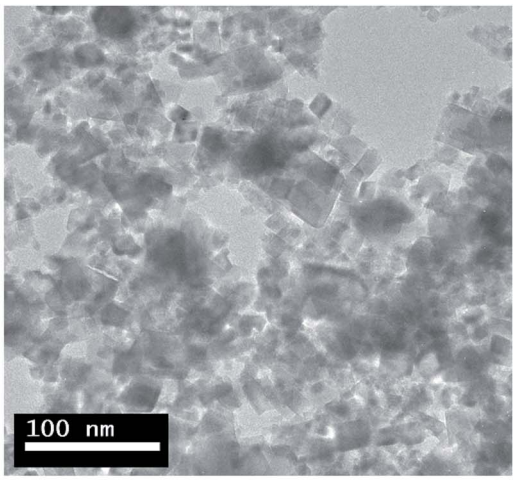

(a)

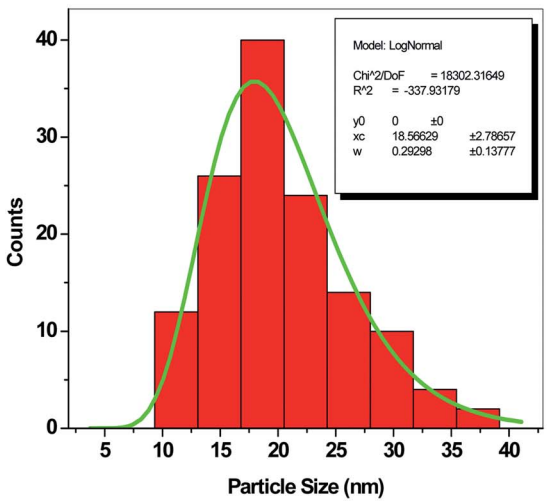

(b)

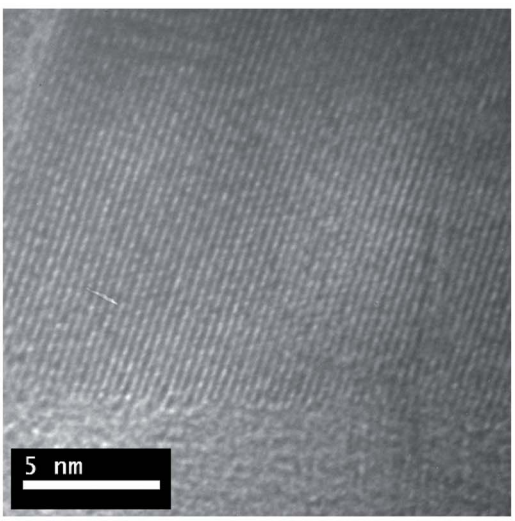

(c)

Fig. 1 High resolution transmission electron micrographs. (a) TEM image of the CeO_2 NPs (b) particle size distribution histogram (w is standard deviation and x_c represents mean particle size ~18.5 nm) (c) HRTEM image of CeO_2 NPs.

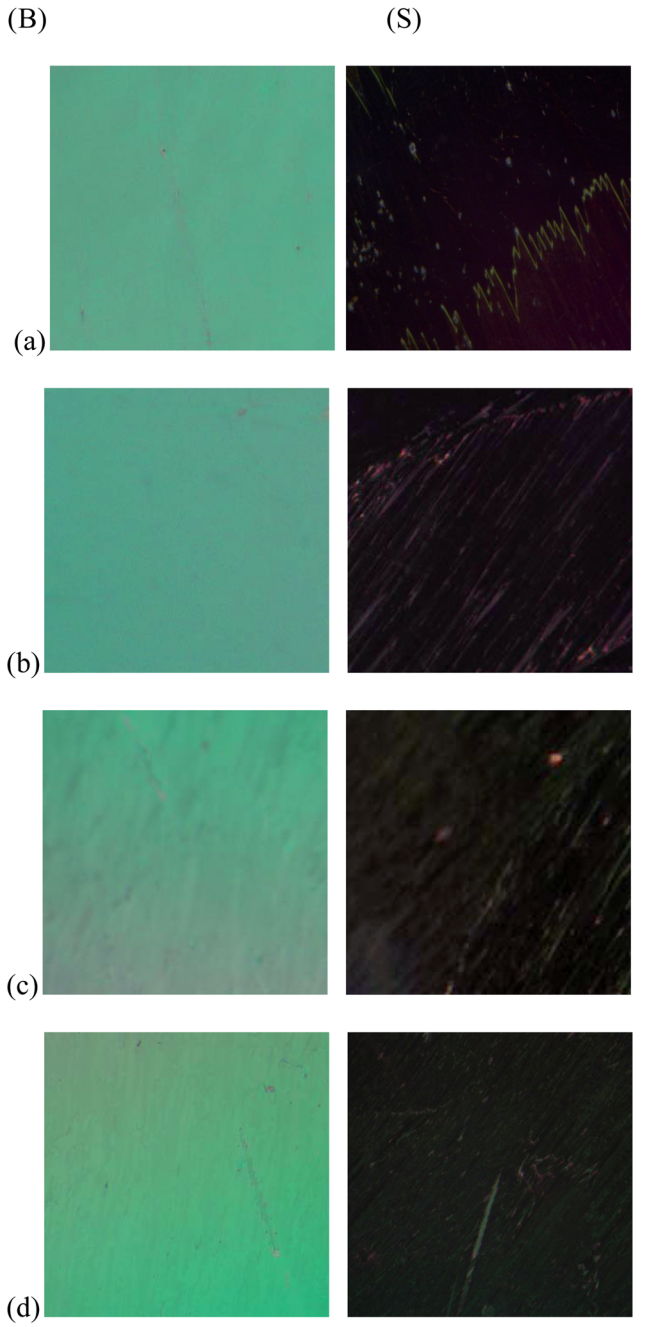

Fig. 2 Polarising optical micrographs of (a) FLC, (b) FLC–0.5% ceria NPs, (c) FLC–1% ceria NPs and (d) FLC-5% ceria NPs. (B) and (S) denote 'bright' and 'scattered/dark' states respectively.

enhancement of the PL signal up to 340 nm excitation. Whereas, a drastic reduction in signal intensity at 370 nm excitation is attributed to the distortion in the layer/helical structure and formation of topological defects in the host FLC material[15] which leads to the saturation of energy levels and thereby negligible energy absorption. As we know, chiral liquid crystals can form self-assembled photonic band gap structures, which can be tuned by external fields. Such structures are realized in the helical cholesteric, the cholesteric blue, the helical ferroelectric and the smectic blue phases. The photonic band gap materials are characterized by classical light propagation being forbidden for

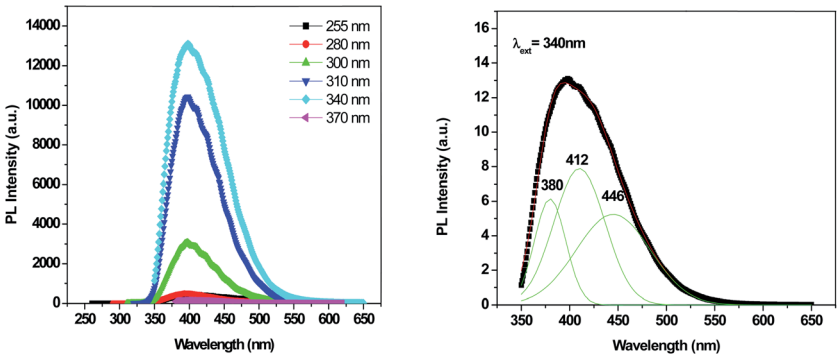

Fig. 3 (a) Emission plots for the FLC material at different excitation wavelengths, (b) the Gaussian fit for the PL peak at 396 nm shows three submerged components at 380, 412 and 446 nm.

some ranges of frequencies because the density of the photon states is suppressed in the stop band and is enhanced at the band edges. This may be the reason for the drastic reduction in the intensity of PL emission at 370 nm which we considered to be the distortions in the layer/helical like structure and the defects formed in the host lattice that act as a stop band.[16]

On the contrary, the PL spectra of pure ceria nanoparticles recorded at different excitation wavelengths (Fig. 4) exhibit a shift in PL maxima to higher wavelengths (red shift) with a broad emission peak. The emission bands originate from the ligand-to-metal charge transfer (LMCT) states O → Ce^{4+} from O_2^{2-} ligand to Ce^{4+} ions *via* hopping of electrons[17] above 3 eV and from the defect levels being localized between the Ce 4f band and O 2p band are the basic reason for a broader emission peak. In CeO_2, the Ce 4f level, with a width of 1 eV, is localized at the forbidden gap (~5.5 eV), which lies at 3 eV over the valence band (O 2p).[8] As shown in Fig. 4, the broad violet emissions with peak maxima in the range of 365 to 400 nm are observed at the excitation wavelengths (255–370 nm) even below the band gap (~5.5 eV) energy of ceria. These emissions are assigned to the electronic transition between the valence band and the Ce 4f level. The red shift of emission peaks *i.e.* from 368 to 396 nm with increasing excitation wavelengths are attributed to the recombination of electrons trapped in the defect band and deeply trapped holes in oxygen vacancies. In addition, the emission intensities shows nonlinear behavior: first increasing, reaching a maximum excitation energy at 340 nm and finally decreasing with negligible emission at 370 nm. The rate of the recombination between photogenerated holes and electrons might be reduced on increasing the excitation wavelength above 340 nm, which leads to the complete quenching of the PL signal in ceria nanoparticles.[18,19]

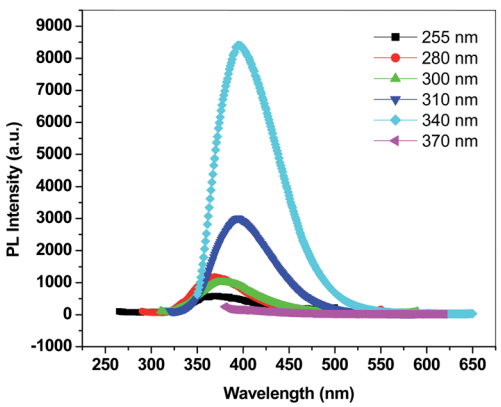

Fig. 4 Emission plots for ceria (CeO_2) NPs at different excitation wavelengths.

Furthermore, to understand the mechanism of excitation wavelength dependent PL peak position and intensity of FLC–ceria nanocomposites, the PL spectra were recorded at excitations of 255 nm, 280 nm, 310 nm and 340 nm. In Fig. 5(a), the characteristics of the PL spectra (at 255 nm excitation) of the nanocomposites were the same as ceria NPs except that the intensity of the PL signals changed with varying ceria concentrations in the FLCs. The violet light emission at the 255 nm excitation corresponds to the emission from the electron transition between Ce 4f → O 2p and defects level → O_2. It is noticeable that the PL signal is enhanced when increasing the ceria nanoparticle concentration to 1 μl and then is quenched on further increasing the dopant concentration to 5 μl. At higher doping concentrations, the NPs dispersed among the FLC are situated relatively close together compared to the lower doping concentration. When this happens, the probability of excitation energy transfer among the NPs will be increased which might serve as a path to non-radiative decay resulting in a quenching of the PL emission. A concentration dependent quenching effect dominates if the energy migration takes places in the time necessary for the radiative decay.[20] Similarly, the emission spectra at 280 nm (Fig. 5(b)) excitation also had the enhancement and quenching effect in nanocomposites with a large blue shift in the spectral energy band of the host FLC. However, a small additional peak appearing at 533 nm (λ_{ext} = 280 nm) corresponds to the excimer luminescence.[21] The efficient interaction of the FLC phenyl rings with ceria NPs *via* hydrogen bonding may lead to the freezing of molecular motion and formation of a predimer state which gives excimer PL (ref. 22) at 280 nm excitation.

In Fig. 5(c, d), where PL spectra were recorded at 310 nm and 340 nm excitations, a strong and broad absorption signal with a

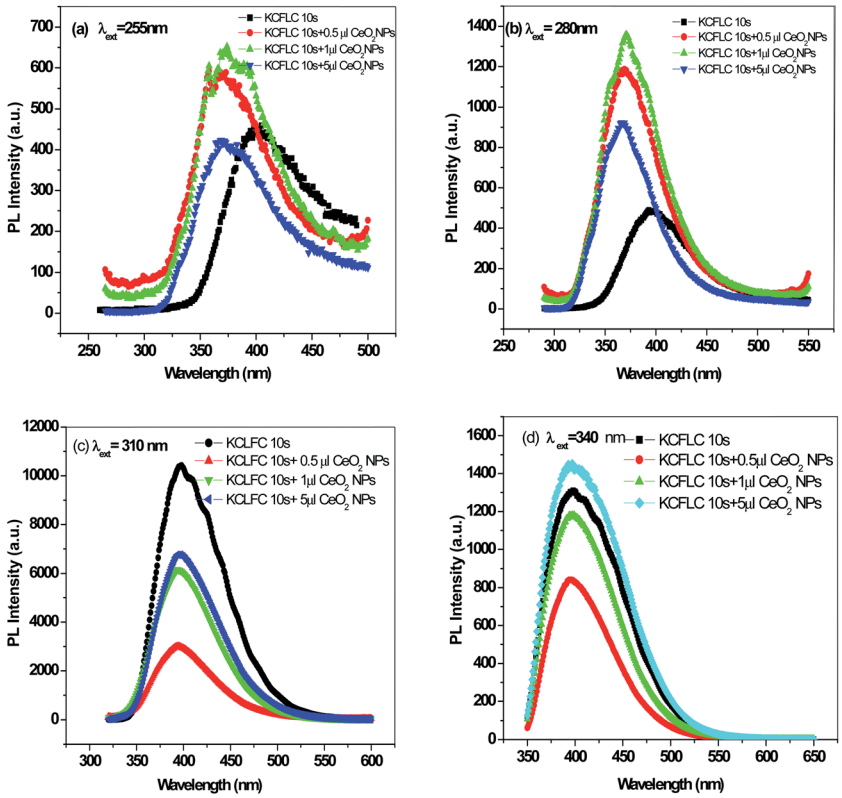

Fig. 5 Emission plots for pure FLC and ceria NPs dispersed samples (a) $\lambda_{ext} = 255$ nm, (b) $\lambda_{ext} = 280$ nm, (c) $\lambda_{ext} = 310$ nm and (d) $\lambda_{ext} = 340$ nm.

peak maximum at 396 nm is observed for the pure FLC as well as ceria doped analogues. At these excitation wavelengths, the 533 nm signal (*i.e.* excimer PL) is absent which might be due to the instability of the predimer states at higher excitation wavelengths. The PL spectra exhibit quenching and enhancement of the emission signal with varying dopant concentration. In 0.5 µl dispersed ceria NP samples, the intensity of the 396 nm emission band was much lower, indicating a quenching of PL emissions. This quenching is due to the alteration of defect bands of ceria in the FLC matrix and overlapping of the emission and absorption band of host FLC and guest ceria NPs. To get a clear understanding of the mechanism playing a role in modifying the PL emissions of the nano-ceria dispersed system, UV-Vis absorption spectra of pure FLC, ceria NPs and all the nanocomposites were recorded in a 200–800 nm range and presented in Fig. 6. One can notice a visible change in the absorption features of FLC–ceria nanocomposites in 280–340 nm range. These features are assigned to the absorption occurring due to the alteration in the defect levels of ceria NPs after dispersing in FLC media. Fig. 7(a) shows the overlapping of the absorption and emission band of the FLC and ceria NPs. The schematic diagram depicting the position of the energy bands of FLCs and ceria NPs is also presented in Fig. 7(b). The enhancement of the PL signal could be observed by increasing the ceria concentration up to 5 µl in these cases. The increase in emission of the PL spectra can be due to the local field enhancement arising from the resonant coupling between the excitons of ceria NPs and FLC molecules as well as the increase in the radiative recombination rate.

Conclusions

The enhancement and quenching in the PL intensity and enormous shift in the spectral energy band of nano-ceria doped FLC nanocomposites have been demonstrated with varying excitation wavelength and ceria concentration. The PL spectra of ceria NPs exhibit atypical excitation wavelength dependence which has been markedly imparted to the host material as well. The spectra recorded at an excitation wavelength where the host liquid crystal and dispersed nanoparticle shows intense absorption, *i.e.* 340 nm, exhibit a quenching effect at lower doping concentration of NPs without any blue/red shift in band

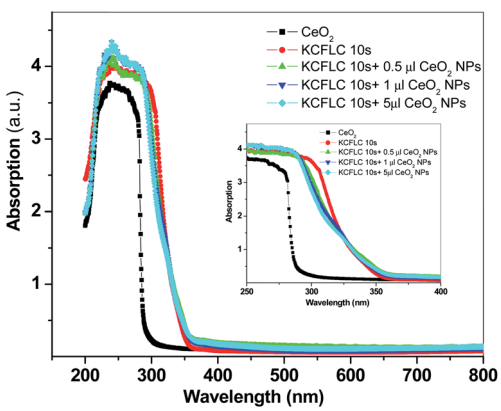

Fig. 6 UV-Vis absorption spectra of ceria NPs, pure FLC and FLC–ceria nanocomposites.

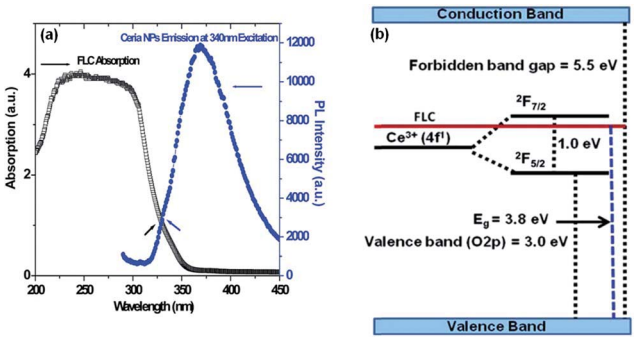

Fig. 7 (a) Overlapping of absorption and emission band of the FLC and ceria NPs. (b) Schematic diagram depicting the tentative structure of band gap energy levels of the FLC and CeO_2 NPs.

position. The quenching in emission intensity has been attributed to the overlapping of the emission and absorption band of the host FLC and guest nanoparticles and the alteration of defect bands of ceria in the FLC matrix. The emission spectra recorded at 255 and 280 nm excitation wavelengths follow a reverse trend: a large blue shift in the spectral energy band of the host material and an increase in the emission intensity at lower concentration of NPs. These studies will provide important information in understanding, designing and tailoring PL properties of FLCs for modern display devices.

Acknowledgements

The authors sincerely thank Professor H. S. Gupta, Director IARI for continuous encouragement and interest in this work. One of the authors (P. Goel) is also thankful to DST, New Delhi for financial support under INSPIRE Faculty Scheme (IFA12-PH-38) and women scientist scheme (SR/WOS-A/Ps-68/2011).

References

1 A. Kumar, J. Prakash, D. S. Mehta, A. M. Biradar and W. Haase, *Appl. Phys. Lett.*, 2009, **95**, 023117.
2 W. A. Crossland, I. D. Springle, R. D. King, P. A. Bayley, A. B. Davey and B. Needham, *Proc. SPIE*, 2002, **3955**, 70.
3 L. J. Yu and M. M. Labes, *Appl. Phys. Lett.*, 1977, **31**, 719.
4 C. Weder, C. Sarwa, A. Montali, C. Bastiaansen and P. Smith, *Science*, 1998, **279**, 835.
5 V. Gayvoronsky, S. Yakunin, V. Pergamenshchik, V. Nazarenko, K. Paleweska, J. Sworakowski, A. Podhorodecki and J. Misiewicz, *Ukr. J. Phys. Opt.*, 2006, **7**, 116.
6 S. Y. Huang, C. C. Peng, L. W. Tu and C. T. Kuo, *Mol. Cryst. Liq. Cryst.*, 2009, **507**, 301.
7 A. Trovarelli, *Catal. Rev.: Sci. Eng.*, 1996, **38**, 439.
8 C. Chunlin, Y. Shaoyan, L. Zhikai, L. Meiyong and C. Nuofu, *Chin. Sci. Bull.*, 2003, **48**, 1198.
9 N. Shehata, K. Meehan, M. Hudait and N. Jain, *J. Nanopart. Res.*, 2012, **14**, 1173.
10 S. Deshpande, S. Patil, S. Kuchibhatla and S. Seal, *Appl. Phys. Lett.*, 2005, **87**, 133113.
11 P. Goel, N. Viajayan and A. M. Biradar, *Ceram. Int.*, 2012, **38**, 3047.
12 B. Liu, X.-L. Hu, J. Liu, Y.-D. Zhao and Z.-L. Huang, *Tetrahedron Lett.*, 2007, **48**, 5958.
13 B.-L. Lee and T. Yamamoto, *Polymer*, 2002, **43**, 4531.
14 M. P. Aldred, A. J. Eastwood, S. P. Kitney, G. J. Richards, P. Vlachos, S. M. Kelly and M. O'Neill, *Liq. Cryst.*, 2005, **32**, 1251.
15 D. P. Singh, S. K. Gupta and R. Manohar, *Adv. Condens. Matter Phys.*, 2013, **2013**, 250301.
16 P. P. Muhoray, W. Cao, M. Moreira, B. Taheri and A. Munoz, *Philos. Trans. R. Soc., A*, 2006, 364, DOI: 10.1098/rsta.2006.1851.
17 E. C. C. Souza, H. F. Brito and E. N. S. Muccillo, *J. Alloys Compd.*, 2010, **491**, 450.
18 A. Kar, S. Kundu and A. Patra, *J. Phys. Chem. C*, 2011, **115**, 118.
19 A. T. de Figueiredo, V. M. Longo, S. de Lazaro, *et al.*, *J. Lumin.*, 2007, **126**, 403.
20 F. Benza and H. P. Strunk, *AIP Adv.*, 2012, **2**, 042115.
21 M. Pope and C. E. Swenberg, *Electronic Processes in Organic Crystals*, Oxford University Press, Oxford, 1982.
22 Y. P. Piryatinskii, O. V. Yaroshchuk, L. A. Dolgov, T. V. Bidna and D. Enke, *Opt. Spectrosc.*, 2004, **97**, 537.